Int. J. Heat Mass Transfer. Vol. 27, No 5, pp. 747 754, 1984
Printed in Great Britain

0017–9310/84 $3.00 + 0.00
Pergamon Press Ltd

THREE-DIMENSIONAL NATURAL CONVECTION IN AN INCLINED CYLINDRICAL ANNULUS

YASUYUKI TAKATA, KENGO IWASHIGE, KENJI FUKUDA and SHU HASEGAWA
Department of Nuclear Engineering, Faculty of Engineering, Kyushu University, Fukuoka 812, Japan

(*Received* 9 *May* 1983 *and in revised form* 30 *July* 1983)

Abstract—An analytical and experimental work is described on natural convection in an inclined cylindrical annulus enclosed in heated inner and cooled outer cylinders. Three-dimensional governing equations are transformed into the finite-difference equations and solved numerically using the successive over-relaxation (SOR) procedure. The three-dimensional structure of the fluid flow and temperature distributions as well as Nusselt numbers are obtained and the effect of inclination on them is examined. A flow visualization experiment using a tracer technique is conducted; photographs of streaklines confirm the three-dimensional flow structure obtained analytically.

NOMENCLATURE

C_p	specific heat
g	gravitational acceleration
l	axial length of the cylinders
L	dimensionless axial length of the cylinders, l/r_2
Nu_1, Nu_2	Nusselt numbers at the inner and the outer cylinder walls defined in equations (19) and (20), respectively
Nu_m	average Nusselt number defined in equation (21)
p_m	dynamic pressure
Pr	Prandtl number, ν/α
r	radial distance
r_1, r_2	inner and outer radii of the annulus, respectively
R	dimensionless radial coordinate, r/r_2
R_1	ratio of the inner to the outer radius, r_1/r_2
Ra	Rayleigh number based on the outer radius, $g\beta(T_1 - T_2)r_2^3/\alpha\nu$
T	temperature
T_1, T_2	temperatures at inner and outer cylinders, respectively
$\mathbf{V}$	velocity vector
z	axial distance.

Greek symbols

α	thermal diffusivity
β	thermal expansion coefficient
δ	angle of inclination from the horizon
θ	dimensionless temperature, $(T - T_2)/(T_1 - T_2)$
ν	kinematic viscosity
ξ	dimensionless axial coordinate, z/r_2
ϕ	angular coordinate measured from downward vertical axis
$\boldsymbol{\Psi}$	vector potential
$\boldsymbol{\Omega}$	vorticity vector.

Subscript

1	inner cylinder
2	outer cylinder.

INTRODUCTION

IN RECENT years, natural convection in a cylindrical annulus has attracted much attention with relation to solar collectors, thermal storage systems and spent nuclear fuel cooling. A review of the works concerning this configuration was presented by Kuehn and Goldstein [1]. However, most of them were for horizontal concentric cylinders with infinite axial length. In this case, a two-dimensional (2-D) analysis is allowed because the convective flow is confined to the vertical plane and the flow pattern is identical in each annular cross section. On the other hand, a three-dimensional (3-D) treatment is unavoidable in the horizontal case with the finite axial length and the rigid axial boundary surfaces and/or in the case when the cylinders are inclined from the horizon, because the viscous shearing force at the end walls and/or the gravitational force have an effect on the convection toward the axial direction.

In the 3-D numerical analysis, the matrix to be dealt with is far larger than that in the 2-D case, taking more CPU time to obtain the solution. Recently it has become feasible to treat this problem due to improvements in processing speed and memory capacity of digital computers. Several numerical works have been performed, most of them for rectangular enclosures. Aziz and Hellums [2] solved numerically a set of transient governing equations for a rectangular configuration by means of an alternating direction implicit (ADI) method. However, their main aim was to find out the possibility of using a vector potential and so the 3-D flow structure was not made clear. Ozoe *et al.* [3] performed a numerical work on 3-D natural convection in a long inclined rectangular box and showed that a fluid particle path drew a co-axial double helix. In later experimental work [4], they confirmed such a flow structure by flow visualization using a tracer technique.

Only a few numerical works have been made on a concentric cylindrical annulus. Ozoe *et al.* [5] carried out analytical and experimental work for a vertical annulus heated from below. In refs. [6, 7] 3-D analytical

and experimental works were performed for a porous medium enclosed in an inclined cylindrical annulus with relation to the insulation of a high temperature ducting system and obtained a good agreement between analytical and experimental temperature distributions. However, the flow structure obtained numerically was not confirmed experimentally because of the difficulty of the flow visualization in a porous medium. As Darcy's law is adopted for the porous layer, the momentum equation is simplified by neglecting small terms; i.e. viscous drag and inertia terms. Consequently the order of the differential equations is less than that for the viscous fluid layer and velocity-slip at the wall is allowed. In spite of this difference it is assumed that the flow structure does not essentially depend so much on the medium but mainly on the geometrical configuration and its boundary conditions. Thus the results in a viscous fluid layer are expected to provide a supplemental confirmation of the flow structure in a porous layer predicted in refs. [6, 7]. The purpose of this paper is to clarify the 3-D flow structure, temperature distributions in a fluid layer as well as Nusselt numbers. The 3-D governing equations in terms of a vector potential, vorticity vector and temperature are solved numerically using an SOR procedure. Furthermore, a flow visualization experiment with grycerol is conducted using suspended aluminum powder as the tracer to confirm the flow structure obtained by numerical analysis.

ANALYSIS

The physical model and the coordinate system in the present analysis are shown in Fig. 1. A fluid layer is enclosed between two concentric cylinders with radii r_1 and r_2, and axial length l. The cylinder axis is inclined from the horizon at an angle δ, and hence the gravitational force acts not only in the r- and ϕ-directions but also in the z-direction. Temperatures at the heated inner cylinder surface and the cooled outer one, designated by T_1 and T_2, respectively, are assumed to be kept constant, while both side walls are thermally insulated. Flow and temperature fields are assumed to have a symmetric nature with respect to the vertical plane ($\phi = 0°$ and $180°$) and the region of computation is limited between $\phi = 0°$ and $180°$. Furthermore, Boussinesq's approximation is applied to the density in the momentum equation and the other properties are assumed to be independent of temperature.

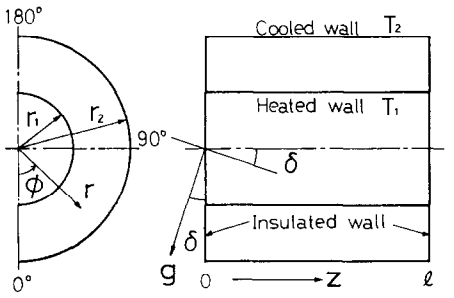

FIG. 1. Analytical model.

Considering these assumptions, the governing equations in the steady state are written as

$$\nabla \cdot \mathbf{V} = 0, \tag{1}$$

$$(\mathbf{V} \cdot \nabla)V = -g\beta(T - T_2)\mathbf{i} - \frac{1}{\rho}\nabla P_m + \nu\nabla^2\mathbf{V}, \tag{2}$$

$$(\mathbf{V} \cdot \nabla)T = \alpha\nabla^2 T, \tag{3}$$

where $\mathbf{i}$ on the RHS of equation (2) represents a unit vector in the direction of the gravitational force and is given, as a function of δ, by

$$\mathbf{i} = \begin{bmatrix} \cos\phi\cos\delta \\ -\sin\phi\cos\delta \\ -\sin\delta \end{bmatrix}. \tag{4}$$

Following Aziz and Hellums [2], the vector potential, $\mathbf{\Psi}$, and vorticity vector, $\mathbf{\Omega}$, are introduced

$$\mathbf{V} = \nabla \times \mathbf{\Psi}, \tag{5}$$

$$\mathbf{\Omega} = \nabla \times \mathbf{V}, \tag{6}$$

where $\mathbf{\Psi}$ and $\mathbf{\Omega}$ satisfy the following solenoidal condition

$$\nabla \cdot \mathbf{\Psi} = 0, \tag{7}$$

$$\nabla \cdot \mathbf{\Omega} = 0. \tag{8}$$

The equation of continuity, equation (1), is satisfied automatically by the vector potential. Then the relation between $\mathbf{\Psi}$ and $\mathbf{\Omega}$ is presented in the following dimensionless form

$$\mathbf{\Omega} = -\nabla^2\mathbf{\Psi}. \tag{9}$$

Taking the curl of equation (2) to eliminate the pressure term, the vorticity transport equation is obtained in the dimensionless form

$$\frac{1}{Pr}\{(\mathbf{V} \cdot \nabla)\mathbf{\Omega} - (\mathbf{\Omega} \cdot \nabla)\mathbf{V}\} = Ra\begin{bmatrix} \sin\delta\dfrac{1}{R}\dfrac{\partial\theta}{\partial\phi} - \sin\phi\cos\delta\dfrac{\partial\theta}{\partial\xi} \\ -\cos\phi\cos\delta\dfrac{\partial\theta}{\partial\xi} - \sin\delta\dfrac{\partial\theta}{\partial R} \\ \cos\delta\left(\sin\phi\dfrac{\partial\theta}{\partial R} + \cos\phi\dfrac{1}{R}\dfrac{\partial\theta}{\partial\phi}\right) \end{bmatrix} + \nabla^2\mathbf{\Omega}. \tag{10}$$

In the same manner, the dimensionless form of the energy equation is written as

$$(\mathbf{V} \cdot \nabla)\theta = \nabla^2\theta. \tag{11}$$

In equations (9)–(11) the following dimensionless variables and parameters are used

$$\left.\begin{aligned} &R = r/r_2, \quad \phi = \phi, \quad \xi = z/r_2, \\ &\theta = (T - T_2)/(T_1 - T_2), \\ &Ra = g\beta(T_1 - T_2)r_2^3/\alpha\nu, \quad Pr = \nu/\alpha. \end{aligned}\right\} \tag{12}$$

Boundary conditions are written as follows.

Velocity:

$$\left.\begin{aligned} &V_R = V_\phi = V_\xi = 0 \quad (R = R_1, 1), \\ &\frac{\partial V_R}{\partial \phi} = V_\phi = \frac{\partial V_\xi}{\partial \phi} = 0 \quad (\phi = 0°, 180°), \\ &V_R = V_\phi = V_\xi = 0 \quad (\xi = 0, L). \end{aligned}\right\} \quad (13)$$

Vorticity:

$$\left.\begin{aligned} &\Omega_R = 0, \quad \Omega_\phi = -\frac{\partial V_\xi}{\partial R}, \quad \Omega_\xi = \frac{\partial V_\phi}{\partial R} \quad (R = R_1, 1), \\ &\Omega_R = \frac{\partial \Omega_\phi}{\partial \phi} = \Omega_\xi = 0 \quad (\phi = 0°, 180°), \\ &\Omega_R = -\frac{\partial V_\phi}{\partial \xi}, \quad \Omega_\phi = \frac{\partial V_R}{\partial \xi}, \quad \Omega_\xi = 0 \quad (\xi = 0, L). \end{aligned}\right\} \quad (14)$$

Vector potential:

$$\left.\begin{aligned} &\frac{\partial}{\partial R}(R\Psi_R) = \Psi_\phi = \Psi_\xi = 0 \quad (R_1 = R_1, 1), \\ &\Psi_R = \frac{\partial \Psi_\phi}{\partial \phi} = \Psi_\xi = 0 \quad (\phi = 0°, 180°), \\ &\Psi_R = \Psi_\phi = \frac{\partial \Psi_\xi}{\partial \xi} = 0 \quad (\xi = 0, L). \end{aligned}\right\} \quad (15)$$

Temperature:

$$\left.\begin{aligned} &\theta = 1 \quad (R = R_1), \quad \theta = 0 \quad (R = 1), \\ &\frac{\partial \theta}{\partial \phi} = 0 \quad (\phi = 0°, 180°), \quad \frac{\partial \theta}{\partial \xi} = 0 \quad (\xi = 0, L), \end{aligned}\right\} \quad (16)$$

where the boundary conditions of the vector potential were developed by Hirasaki and Hellums [8]. Equations (5) and (9)–(11) are the final forms of the governing equations, which were transformed into the finite-difference equations and solved numerically using an SOR procedure with the parameters δ and Ra. Computations were carried out in the ranges of $0° \leqslant \delta \leqslant 90°$, $10^4 \leqslant Ra \leqslant 10^5$ and $Pr = 5000$ with fixed aspect ratios of $R_1 = r_1/r_2 = 0.5$ and $L = l/r_2 = 2$. As an initial condition of the iteration, a conduction solution was adopted for the temperature distribution, while the zeroes were substituted into the remaining unknowns. Iterations were terminated when the following relative-error convergence criterion was satisfied

$$\text{Max}\left|\frac{Q_{i,j,k}^{(n+1)} - Q_{i,j,k}^{(n)}}{Q_{i,j,k}^{(n)}}\right| \leqslant 10^{-3}, \quad (17)$$

where $Q_{i,j,k}^{(n)}$ indicates one of the values Ω, Ψ or θ at the nth step of the iterations at a location (R_i, ϕ_j, ξ_k). For a higher value of Ra, the solution obtained for smaller Ra was used as the initial condition to save CPU time. It took 17–220 min to obtain a convergence solution using a FACOM M-200 digital computer. The relaxation factors chosen were in the ranges 0.8–1.0 for the vorticity and 1.0–1.2 for the vector potential and the temperature, and the number of nodal points in the grid was 21, 37, and 41 for the R-, ϕ-, and ξ-directions, respectively.

EXPERIMENTAL APPARATUS AND PROCEDURE

The experimental apparatus for flow visualization is shown in Fig. 2. The inner cylinder was made of phenol resin with a diameter of 45 mm and covered with stainless steel foil for electrical heating, which was coated with black flat paint to prevent reflection of light. The outer cylinder was made of a Pyrex glass tube, 90 mm I.D., to make the inside visible and cooled outside by water. The gap between the outer cylinder and the flat viewing window was filled with cooling water to reduce the refraction by curvature of the outer cylinder. Two end plates were made of acrylic resin. Some rubber corks, through which the tracer was injected, were attached to these end plates. Temperatures on the inner and outer cylinder surfaces were measured by chromel–alumel thermocouples. Grycerol was used as the test fluid, while suspended aluminum powder was used as the tracer. Usually it took more than 30 h to attain steady state. Photographs of the flow patterns were taken and a video tape recorder unit was used to record the tracer particle movement.

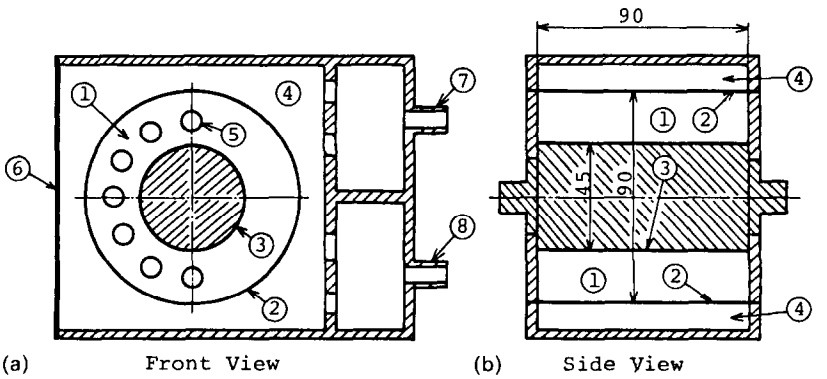

FIG. 2. Experimental apparatus: (a) front view; (b) side view. (1) Test section; (2) cooled outer cylinder; (3) heated inner cylinder; (4) water jacket; (5) rubber cork; (6) window; (7) inlet; (8) outlet.

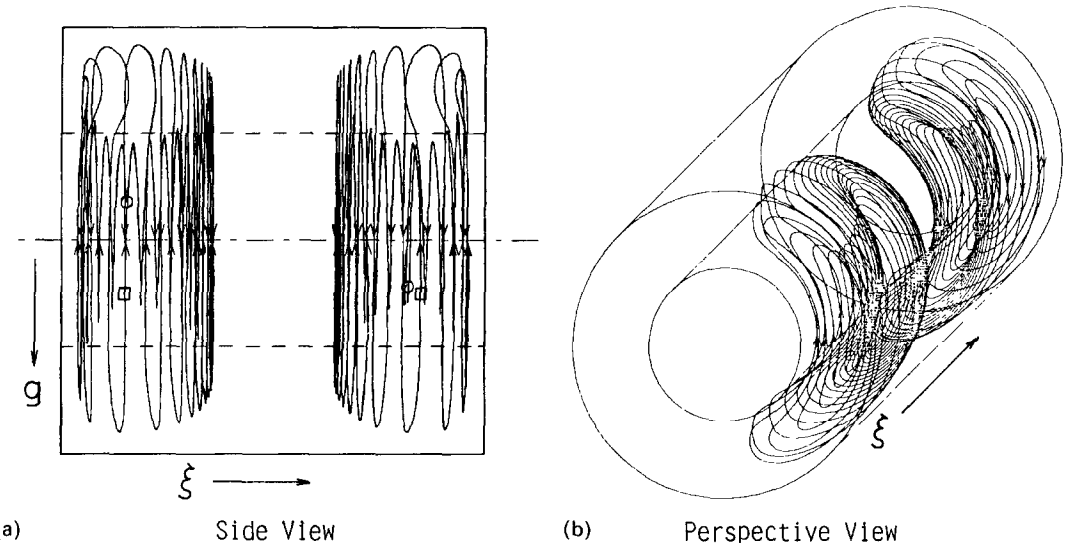

FIG. 3. Fluid particle path for $\delta = 0°$, $Ra = 10^4$ and $Pr = 5000$: (a) side view; (b) perspective view.

RESULTS AND DISCUSSION

Horizontal case

The stream line draws an almost 2-D crescent-shaped vortex as obtained by Kuehn and Goldstein [1] even if both of the axial boundary surfaces are rigid. The problem may be treated as 2-D one as far as convection in the R–ϕ plane is concerned. However, the effect of the viscous shearing force at the end walls manifests itself in the region very close to the walls and in the middle part of the annulus. Figure 3 shows fluid particle paths for the horizontal case at $Ra = 10^4$ and $Pr = 5000$, which is obtained by numerical integration of the following differential equation by means of the Runge–Kutta method of the second order

$$\frac{dR}{V_R} = \frac{Rd\phi}{V_\phi} = \frac{d\xi}{V_\xi} = dt. \tag{18}$$

Two fluid particle paths, whose starting and ending points are marked by square and circular symbols, respectively, are shown in the figure. Referring to the left-hand path, the fluid particle moves in the ξ-direction from the starting point, drawing a small crescent-shaped vortex in the R–ϕ plane, but the particle velocity in the ξ-direction decreases gradually at the central region with an increase in the size of the crescent-shape. Then the particle turns in the opposite ξ-direction and moves drawing a large crescent-shaped vortex outside the smaller one. Finally it returns to the starting point. Therefore, such a trace of a fluid particle is closed three-dimensionally and called a co-axial double helix, which is essentially the same structure as that obtained by Ozoe *et al.* [3] for an inclined rectangular box. Since, for the horizontal case, the system is symmetric with respect to the central vertical plane ($\xi = 1$), a couple of the double helixes with the opposite ξ-direction exist. For $Ra = 10^5$ (not shown here) this configuration did not change substantially. As Ra increases, the convection in the R- and ϕ-directions becomes more dominant and it results in decreasing the velocity of the ξ component. The fluid particle is, then, required to draw a larger number of crescent-shaped traces until it returns to the starting point; consequently it becomes more difficult to distinguish each line.

Figure 4 shows the isothermal lines at $\xi = 0$ and 1 for $Ra = 10^5$ and $Pr = 5000$. Each contour line is drawn at a temperature step of 0.1. It is shown that the isothermal lines are concentrated at the lower part of the inner cylinder and at the upper part of the outer one. The lines near $\phi = 180°$ at $\xi = 1$ spread more widely toward the outside compared with those at $\xi = 0$. This is due to the fact that the convection is suppressed by the viscous shearing force at the end wall.

Distributions of local Nusselt numbers corresponding to the isothermal lines are shown in Fig. 5, where Nu_1 represents the value at the inner cylinder wall and Nu_2 at the outer. They are evaluated by the following

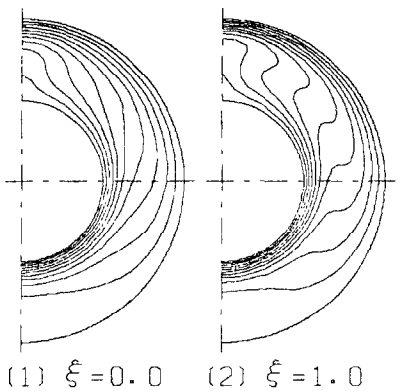

FIG. 4. Isothermal lines on the R–ϕ plane for $\delta = 0°$, $Ra = 10^5$ and $Pr = 5000$.

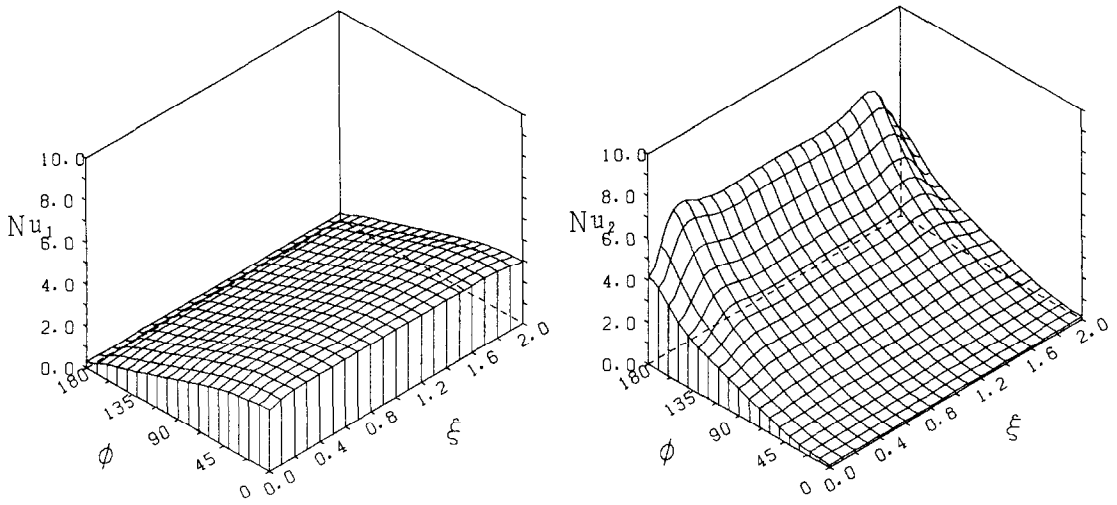

FIG. 5. Local Nusselt numbers, Nu_1 and Nu_2, for $\delta = 0°$, $Ra = 10^5$ and $Pr = 5000$.

expressions

$$Nu_1 = R_1 \ln R_1 \left(\frac{\partial \theta}{\partial R}\right)_{R=R_1}, \tag{19}$$

$$Nu_2 = \ln R_1 \left(\frac{\partial \theta}{\partial R}\right)_{R=1}. \tag{20}$$

From the figure it is found that Nu_1 changes little along the ξ-direction; the values at both of the end walls are almost the same as that at the center. On the other hand, Nu_2 decreases remarkably at both of the end walls ($\xi = 0$ and 2), which is reduced by as much as 30% that of the center and has maxima at $\xi = 0.25$ and 1.75, $\phi = 180°$. This result shows that the end wall does not so much affect the heat transfer characteristics at the inner cylinder but at the outer. As shown in the figure the end effect is very small in the range $0.4 \leqslant \xi \leqslant 1.6$, where 2-D analysis may give a good approximation.

Inclined case

Figure 6 shows a fluid particle path for $\delta = 15°$, $Ra = 10^4$ and $Pr = 5000$. The co-axial double helix is also shown here, but owing to the inclination the velocity in the ξ-direction is fairly large. Referring to the inside helix, the fluid particle flows almost parallel to the vertical line. On the other hand, the outside particle moves back and forth in the ξ-direction in the upper and the lower part of the annulus, drawing a twisted crescent-shaped helix. Figure 7 shows a photograph of streaklines obtained by a flow visualization experiment for $\delta = 15°$, $Ra = 1.5 \times 10^5$ and $Pr = 5156$. Comparing this photograph with Fig. 6, one finds remarkable consistency between them. Thus the structure of the co-axial double helix obtained analytically was confirmed.

Figure 8 shows contour lines of the temperature distribution for $\delta = 15°$ and $Ra = 10^5$. It is shown that its variation with the value of ξ is remarkably large. Isothermal lines gather around the inner cylinder at $\xi = 0$. As the value of ξ increases, the inner lines in the upper part of the annulus spread toward the outside. The corresponding local Nusselt numbers are shown in Fig. 9. The effect of inclination on the distribution of Nu_1 and Nu_2 appear at the end region: one can find the increase in Nu_1 and the decrease in Nu_2 at the bottom end ($\phi = 180°$, $\xi = 0$), and the increase in Nu_2 at the top end ($\phi = 180°$, $\xi = 2$).

The values of the maximum local Nusselt numbers, $Nu_{1,\max}$ and $Nu_{2,\max}$, and average Nusselt number, Nu_m, are listed in Table 1. The average Nusselt number, Nu_m, is defined by

$$Nu_m = \frac{1}{\pi L} \int_0^L \int_0^\pi Nu_1 \, d\phi \, d\xi = \frac{1}{\pi L} \int_0^L \int_0^\pi Nu_2 \, d\phi \, d\xi. \tag{21}$$

The value of Nu_m calculated by Nu_1 agreed with that calculated by Nu_2 within 0.1%. From Table 1, in the

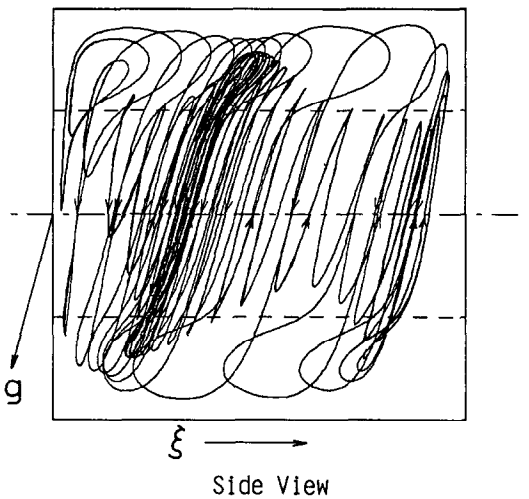

FIG. 6. Fluid particle path for $\delta = 15°$, $Ra = 10^4$ and $Pr = 5000$ (side view).

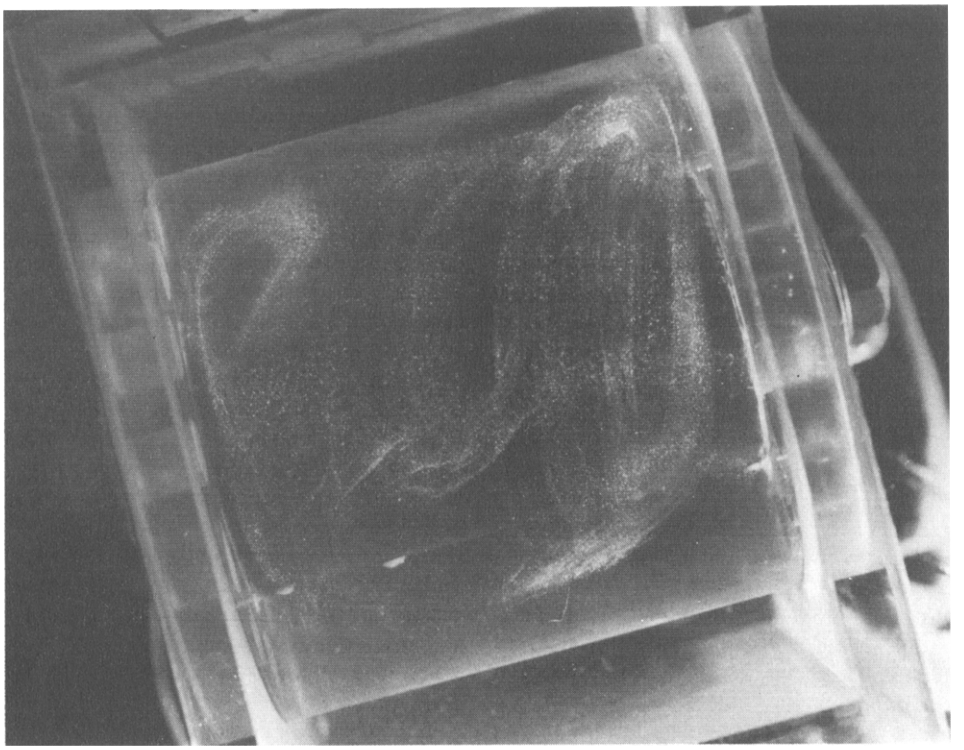

FIG. 7. Photographs of the fluid particle path for $\delta = 15°$, $Ra = 1.5 \times 10^5$ and $Pr = 5156$.

present aspect ratios ($r_1/r_2 = 0.5$ and $l/r_2 = 2$) it is shown that the average Nusselt number slightly increases with δ and attains a maximum value at $\delta = 90°$ (vertical case); the value is higher than at $\delta = 0°$ (horizontal case) by 13%. On the other hand, the maximum local Nusselt numbers, $Nu_{1,max}$ at the inner cylinder wall and $Nu_{2,max}$ at the outer cylinder wall, have their maximum values at $\delta = 75°$ and 60°, respectively, in most cases at locations $\phi = 0°$, $\xi = 0$ (bottom end) for $Nu_{1,max}$, and $\phi = 180°$, $\xi = 2$ (top end) for $Nu_{2,max}$. For a small inclination ($\delta \leqslant 15°$) the location of $Nu_{2,max}$ slightly deviates from $\xi = 2$ because of the end effect. In spite of the apparently large effect of δ on the local Nusselt number distribution, the average Nusselt number changes only slightly. It seems that the effect of the locally promoted or suppressed part of the convection on the total heat transfer rate almost compensates each other. Above results are limited to the case of $r_1/r_2 = 0.5$ and $l/r_2 = 2$. In general, it is considered that the average Nusselt number and local maximum Nusselt numbers depend not only on the inclination but also on the aspect ratios. Additional calculations with the aspect ratios are, of course, necessary for clarifying the whole effects of the inclination.

CONCLUDING REMARKS

A problem of 3-D natural convection in an inclined cylindrical annulus heated from the inner cylinder and cooled from the outer was examined by numerical

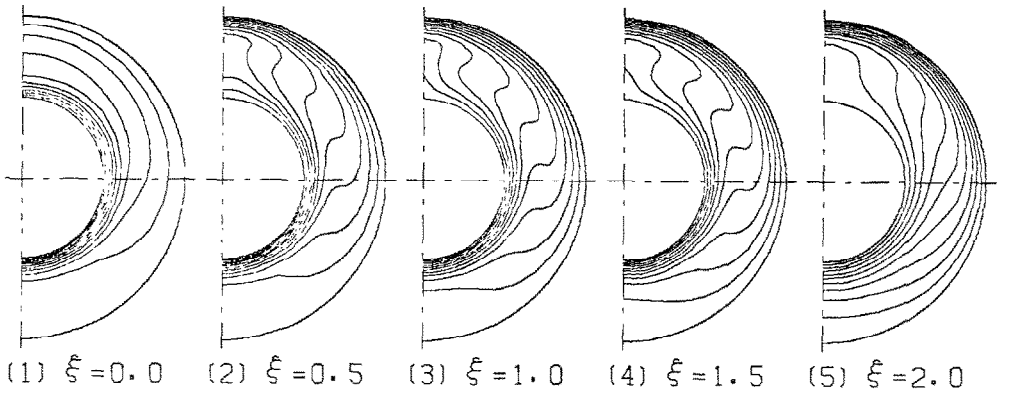

FIG. 8. Isothermal lines on the R–ϕ plane for $\delta = 15°$, $Ra = 10^5$ and $Pr = 5000$.

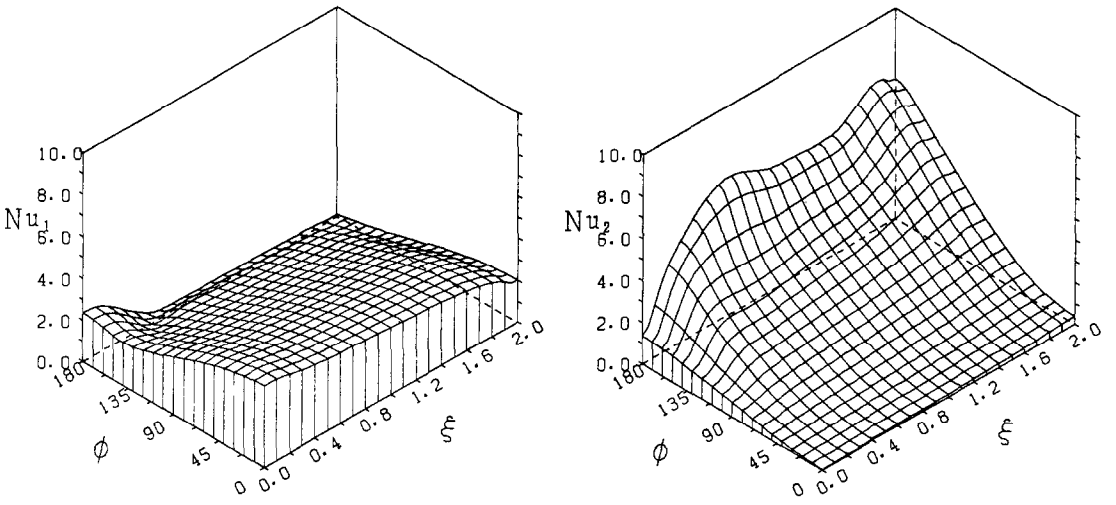

FIG. 9. Local Nusselt numbers, Nu_1 and Nu_2, for $\delta = 15°$, $Ra = 10^5$ and $Pr = 5000$.

analysis and a flow visualization experiment. The conclusions are summarized as follows:

(1) The 3-D structure of the fluid particle path is the coaxial double helix. A streakline obtained by the flow visualization experiment shows a remarkable consistency with the numerical result.

(2) In the limited case of $r_1/r_2 = 0.5$ and $l/r_2 = 2.0$, the average Nusselt number slightly increases as the inclination increases. On the other hand, the maximum local Nusselt numbers show a fairly large dependence on the inclination angle. In the present case, the maximum local Nusselt numbers, $Nu_{1,\max}$ at the inner cylinder and $Nu_{2,\max}$ at the outer cylinder, have maxima at $\delta = 75°$ and 60°, respectively.

(3) In most cases, the locations where the local Nusselt numbers, Nu_1 at the inner cylinder and Nu_2 at the outer cylinder, have maxima are at the top and the bottom end walls, respectively. For a small inclination ($\delta \leqslant 15°$), its location deviates from the end walls because of the viscous shearing force effect at the end.

REFERENCES

1. T. H. Kuehn and R. J. Goldstein, An experimental and theoretical study of natural convection in the annulus between horizontal concentric cylinders, *J. Fluid Mech.* **74**, 695–719 (1976).
2. K. Aziz and J. D. Hellums, Numerical solution of the three-dimensional equations of motion for laminar natural convection, *Physics Fluids* **10**(2), 314–324 (1967).
3. H. Ozoe, K. Yamamoto, H. Sayama and S. W. Churchill, Natural convection patterns in a long inclined rectangular box heated from below, *Int. J. Heat Mass Transfer* **20**, 131–139 (1977).
4. H. Ozoe, N. Sato and S. W. Churchill, Experimental confirmation of the three-dimensional helical streaklines previously computed for natural convection in inclined rectangular enclosures, *Int. Chem. Engng* **19**(3), 454–462 (1979).
5. H. Ozoe, T. Okamoto and S. W. Churchill, Natural convection in a vertical annular space heated from below, *Heat Transfer—Jap. Res.* **8**, 82–93 (1979).
6. K. Fukuda, Y. Takata, S. Hasegawa, H. Shimomura and K. Sanokawa, Three-dimensional natural convection in a porous medium between concentric inclined cylinders, *Proc. 19th Natl Heat Transfer Conf.*, Vol. HTD-8, pp. 97–103 (1980).
7. Y. Takata, K. Fukuda, S. Hasegawa, K. Iwashige, H. Shimomura and K. Sanokawa, Three-dimensional natural convection in a porous medium enclosed with concentric inclined cylinders, *Proc. 7th Int. Heat Transfer Conf.*, Vol. 2, pp. 351–356 (1982).
8. G. J. Hirasaki and J. D. Hellums, A general formulation of the boundary conditions on the vector potential in three-dimensional hydrodynamic, *Q. Appl. Math.* **26**(3), 331–342 (1968).

Table 1. Variation of average Nusselt numbers, Nu_m, and local maximum Nusselt numbers, $Nu_{1,\max}$ and $Nu_{2,\max}$, with inclination at $Ra = 10^5$, $Pr = 5000$, $r_1/r_2 = 0.5$ and $l/r_2 = 2.0$

δ (deg.)	Nu_m	$Nu_{1,\max}$	(ϕ, ξ)	$Nu_{2,\max}$	(ϕ, ξ)
0	2.0734	3.2328	(0, 1.0)	6.7694	(180, 0.25)
15	2.1085	3.8760	(0, 0.1)	7.0526	(180, 1.9)
30	2.1609	4.6212	(0, 0.0)	8.0996	(180, 2.0)
45	2.2297	5.1415	(0, 0.0)	8.8825	(180, 2.0)
60	2.2945	5.4490	(0, 0.0)	9.0325	(180, 2.0)
75	2.3370	5.5566	(0, 0.0)	8.6256	(180, 2.0)
90	2.3513	5.4674	(0, 0.0)	7.6779	(180, 2.0)

CONVECTION TRIDIMENSIONNELLE NATURELLE DANS UN ESPACE ANNULAIRE INCLINE

Résumé—On décrit un travail analytique et expérimental sur la convection naturelle dans un espace annulaire incliné entre un cylindre intérieur chauffé et un cylindre extérieur froid. Les équations tridimensionnelles sont transformées en des équations aux différences finies et elles sont résolues numériquement en utilisant la méthode de surelaxations successives (SOR). La structure tridimensionnelle de l'écoulement et les distributions de température et des nombres de Nusselt sont obtenues et l'effet de l'inclinaison est étudié. Une visualisation expérimentale par une technique de traceur est réalisée: des photographies confirment la structure tridimensionnelle de l'écoulement obtenue analytiquement.

DREIDIMENSIONALE NATÜRLICHE KONVEKTION IN EINEM GENEIGTEN ZYLINDRISCHEN RINGRAUM

Zusammenfassung—Es wird eine theoretische und experimentelle Arbeit beschrieben, die sich mit der natürlichen Konvektion in einem geneigten zylindrischen Ringraum befaßt, wobei der innere Zylinder beheizt und der äußere Zylinder gekühlt ist. Die bestimmenden dreidimensionalen Gleichungen werden in finite Differenzengleichungen transformiert und numerisch gelöst, wobei die sukzessive Überrelaxationsmethode (SOR) angewandt wird. Dabei werden die dreidimensionale Struktur der Geschwindigkeits- und Temperaturverteilung sowie die Nusselt-Zahlen erhalten, und der Einfluß der Neigung auf diese Größen wird untersucht. Die Strömung wurde mit einem Tracer-Verfahren sichtbar gemacht; Fotografien der Streichlinien bestätigen die berechnete dreidimensionale Strömungsstruktur.

ТРЕХМЕРНАЯ ЕСТЕСТВЕННАЯ КОНВЕКЦИЯ В КОЛЬЦЕВОМ ЗАЗОРЕ МЕЖДУ НАКЛОННЫМИ ЦИЛИНДРАМИ

Аннотация—Представлены результаты аналитического и экспериментального исследования естественной конвекции в кольцевом зазоре между наклонными нагреваемым внутренним и охлаждаемым внешним цилиндрами. Трехмерные уравнения естественной конвекции преобразованы в конечно-разностные и решены численно с использованием метода верхней релаксации. Получена трехмерная структура распределений скорости жидкости и температуры, а также определены значения числа Нуссельта и исследовано влияние на них наклона. Течение в зазоре визуализировалось с помощью химического индикатора; фотографии штриховых линий подтверждают трехмерный характер структуры потока, полученный аналитически.